Reynolds number dependence of the structure functions in homogeneous turbulence

John Kaminsky[1], Björn Birnir[1,3], Gregory P. Bewley[2],
and Michael Sinhuber[4]
CNLS and Department of Mathematics
UC Santa Barbara[1], University of Iceland[3],
Department of Mechanical Engineering
Cornell University[2], and
Department of Civil and Enviromental Engineering
Stanford University[4].

Abstract

We compare the predictions of the stochastic closure theory (SCT) [5] with experimental data, obtained in the Variable Density Turbulence Tunnel (VDTT) [8], at the Max Planck Institute for Dynamics and Self-Organization in Göttingen. Given a mean flow in homogeneous turbulence the comparison with the data reduces the number of parameters in SCT to just three, one characterizing the variance of the mean field noise and another characterizing the rate in the large deviations of the mean. The third parameter is the decay exponent of the Fourier variables in the Fourier expansion of the noise. This characterizes the smoothness of the turbulent velocity.

We compare the data for the even structure functions ranging from the the second to the eight structure function and the third structure function, to the SCT theory with generic noise, depending on the above three parameters, with five Taylor-Reynolds (T-R) numbers ranging from 110 to 1450. The theory gives excellent comparison with data for all the structure functions, for all the Taylor-Reynolds numbers. This highlights the advantage of the SCT theory, where the structure functions can be computed explicitly and their dependance on the T-R number computed. These results are robust with respect to the size of the dissipation range filters, applied to the data, and

comparison with the fits without the T-R number corrections, shows a clear improvement with the corrections present. This improvement is significant for the lower T-R number and disappears as the T-R number becomes large, as expected.

Very surprisingly the comparison of SCT and the data also gives information about the smoothness of the turbulent velocity as T-R becomes very large.

1 Introduction

In Aeronautics the design of airfoils and airplanes was originally a major challenge. There was a lack of experiments designed and performed under laboratory conditions and this hampered progress on such designs. The development of the wind tunnel turned out to be the major breakthrough in creating the necessary experiments. The first wind tunnel is credited to F. Wenham in Great Britain in 1871, the Wright brother also made their own wind tunnel in 1901 [2], but it was Ludwig Prandtl in 1917 who designed the first "modern" wind tunnel. This wind tunnel was actually his second design. In 1909, he designed the first closed-loop wind tunnel, but it was, by his own admission, "of a temporary nature" [19]. Thus, a more permanent design was made which would become the foundation for all subsequent wind tunnels [1]. Prandtl's student, Max Munk, would go on to design the first wind tunnel which allowed an adjustment of the density of the working fluid [8], allowing for a much higher Reynolds number flow in the tunnel. This tunnel was built in at the Langley Research Center in Virgina in 1923. However, most of the research done by Prandtl and others working with wind tunnels was devoted to studying airfoils and airplane shapes [8].

In addition to being the perfect tool to study airfoils and model airplanes, wind tunnels are ideal for the creation of statistically homogeneous and isotropic turbulence, see Taylor [23], in an experimental setting. Such a flow limits turbulence to its essential ingredients: inertia, pressure and friction, minimizes the effects of the boundaries on the flow and does not exhibit a preferred orientation. It can be created by mechanically stirring a liquid or gas [8]. A close approximation of such flows are realized in a wind tunnel when a uniform free-stream flow is disturbed by a mesh or a grid, see [10, 9].

Experiments performed to study homogeneous or more general turbulence were rare until the second half of the twenthieth century. The 1960s featured an experiment on grid turbulence in California, while another series of experi-

ments were performed at the Nuclear Research Lab in Jülich in the 1970s. More recently, wind tunnels were built at the German Aerospace Center in Göttingen and at the Princeton Gas Dynamics Lab with the goal of studying turbulence. The facility where the experiments in this paper where performed, the Variable Density Turbulence Tunnel (VDTT) at the Max Planck Institute for Dynamics and Self-Organization in Göttingen, was completed in 2009, see [8]. It has achieved turbulent flow up to Taylor-Reynolds number 1600, which is the highest recorded for a grid experiment. Details about the VDTT can be found in [8]. One of Prandtl's original wind tunnels sits besides the VDTT in Göttingen, see [8].

In this paper, we will examine the structure functions of turbulence coming from data obtained in the VDTT. We will compare with the stochastic closure theory in [6] and show that the Reynolds number dependence of the data is captured by this theory originally published in [5]. More surprisingly, we obtain unexpected results on the smoothness of the flow velocity, in homogenous turbulence, from the data.

The mathematical theory of turbulence has its roots in the work of Kolmogorov. In 1941, Kolmogorov published his celebrated four-fifths law and postulated, with Obukhov, that the structure functions of turbulence should scale with lag variable, i.e.

$$S_p(x,y,t) = E(|u(x,t) - u(y,t)|^p) = C_p r^{\frac{p}{3}},$$

where p is the number of the structure function and $r = |x-y|$. Lev Landau would immediately criticize this theory for not taking into account the influence of the large scale flow structure and the influence of intermittency, the development of long tails in the velocity difference distributions at large Reynolds numbers. In 1962, Kolmogorov and Obukhov revised their theory to address these criticisms. They introduced a correction term to the exponent, i.e.

$$S_p(x,y,t) = C_p < \varepsilon^{\frac{p}{3}} > r^{\frac{p}{3}} = C'_p r^{\frac{p}{3}+\tau_p} = C'_p r^{\zeta_p},$$

where ε is the dissipation rate and $\zeta_p = \frac{p}{3} + \tau_p$. The exact form of this correction was found by She and Leveque in 1994 to be

$$\tau_p = -\frac{2p}{9} + 2(1 - (\frac{2}{3})^{\frac{p}{3}}), \tag{1}$$

see [21]. In [5], the log-Possonian processes of Dubrulle [11] and She and Waymire [22], responsible for the intermittency corrections, were derived from the stochastic Navier-Stokes equation.

Kolmogorov and Obukhov considered the velocity in turbulent flow to be a stochastic process and their hypothesis can be interpreted to say, see [18], that the N-point probability distribution function (PDF) of turbulence does not depend on x or y individually but only on r and ν and ε. Moreover, when $r >> \eta$, where η is the Kolmogorov (dissipation) scale, then the PDF only depends on ε and r and is independent of the viscosity ν. Since the 2-point PDF determines the structure functions the same statements apply to them.

If the turbulent velocity is a stochastic process it must satisfy a stochastic Navier-Stokes equation and such an equation was formulated by Landau and Lifschitz in their Fluid Dynamics book [15] in 1959. They considered the noise in the stochastic Navier-Stokes equation to be the fluctuations in the fluid, that cannot be ignored in fully developed turbulence, and argued that is should be white both in time and space. The latter assumption cannot be true, the Navier-Stokes equation driven by noise that is white in space produces velocities the are not continuous in three dimensions, see [24], and this is not observed in nature. Birnir [5] argued that the noise had have enough smoothness in space so that the dissipation rate ε was finite and be of a generic nature, including an additive term corresponding to a mean-field noise and another corresponding to the large deviations of the mean-field. He also added a multiplicative noise term, modeling jumps in the gradient for the flow velocity, and was able to show that this term produced the log-Poisson processes of Dubrulle, She and Waymire and their intermittency corrections τ_p. These assumptions are the basis of the Stochastic Closure Theory (SCT) [6].

2 The Assumptions of SCT and Its Predictions

The Stochastic Closure Theory (SCT) is based on the following assumptions:

SCT Assumptions:

1. The small scale flow in fully developed turbulence satisfies a stochastic Navier-Stokes (SNS) equation.

2. The noise in the SNS consists of both an additive and a multiplicative term.

3. The additive noise term is a general mean field noise that has enough spatial smoothness for the dissipation rate

$$\varepsilon = \nu \int_\Omega |\nabla u|^2 dx < \infty,$$

to be finite. In addition to this "infinite-dimensional Brownian" mean-field noise, there is a deterministic additive term that estimates the large-deviations of the mean-field.

4. The multiplicative noise term consists of pure jumps, modeling jumps in the velocity gradient ∇u, multiplied by the velocity u.

5. The most singular (having least spatial smoothness) structures in (3-d) turbulence are one-dimensional vortex lines.

These assumptions produce the Stochastic Navier-Stokes equation (5) below. The detailed arguments leading to the form of the noise are given in [5] and [6]. They follow the spirit of the argument in Landau and Lifschitz [15].

The predictions of the SCT theory is the Kolmogorov-Obukhov '62 theory of turbulence, with the She-Leveque intermittency corrections, in all quantitative detail. In particular,

SCT Predictions:

1. The structure functions of turbulence are given by explicit formulas.

2. The Reynolds number dependence of the structure functions is also given explicitly.

3. The N-point probability density functions of turbulence exists and can be computed. In the 2-point case, it is determined by the Kolmogorov-Hopf functional differential equation, see [6], and has an explicitly formula, see [7].

4. The PDF for the velocity distribution in turbulence is a Generalized-Hyperbolic distribution [3] convolved with the Poisson distribution of the log-Poisson processes of Dubrulle, She and Waymire, see [7].

The most important SCT prediction for this paper is number 2, that we have an explicit formula for the structure functions with their Reynolds number dependence given. This means that we can use these formulas to fit the data measured in the VDTT and this is the subject of the paper. The disadvantage when we consider equation (5) is that the noise has infinitely many undetermined coefficients c_k, d_k and h_k. The last coefficients are fixed by the assumption number 4 above. Namely, that the vorticity lines are one-dimensional implies that all the

coefficients h_k are fixed, see [6]. But we are still left with infinitely many coefficients c_k, d_k. The miraculous fact is that the comparison with the VDTT data reduces these coefficients to only three. When the mean flow is given, we get one parameter characterizing the infinite-dimensional Brownian, another parameter characterizing the large deviation of the mean and one power characterizing both, or their spatial smoothness. Of course the mean flow and these three parameters depend on the Taylor-Reynolds number but not on the order of the structure functions. The upshot is a much improved stochastic closure model (18) with only three parameters characterizing the noise.

3 The Stochastic Closure Model and the Structure Functions

In this section, we describe the calculation of the structure functions of turbulence, which will be compared with the experimental data. The flow in the wind tunnel is governed by the Navier Stokes equation:

$$\begin{aligned} u_t + (u\cdot\nabla)u &= \nu\Delta u - \nabla p, \\ \operatorname{div} u &= 0, \\ u(x,0) &= u_0(x), \end{aligned} \tag{2}$$

where $u(x)$ is the fluid velocity, $x \in \mathbb{R}^3$, p is pressure, and ν is the viscosity. The second line in (2) is the incompressibility condition. Using the incompressibility, we can eliminate the pressure to get

$$u_t + u\cdot\nabla u = \nu\Delta u + \nabla(\Delta^{-1}[\mathrm{Trace}(\nabla u)]^2). \tag{3}$$

This equation defines the small scale velocity flow, or the fluctuations in the mean of the flow. We will impose periodic boundary conditions on the small scales below.

Following the classical Reynolds decomposition [20], we decompose the velocity into mean flow U and the fluctuations u. Then the velocity is written as $U+u$, where U describes the mean, or large scale flow and u describes the velocity fluctuations. These two terms describe the large scales and small scales of the flow, respectively. We must also decompose the pressure into mean pressure P and the fluctuations p, then the equation for the large scale flow can be written as

$$U_t + U\cdot\nabla U = \nu\Delta U - \nabla P - \nabla\cdot(\overline{u\otimes u}), \tag{4}$$

where in coordinates $\nabla \cdot (\overline{u \otimes u}) = \frac{\partial \overline{u_i u_j}}{\partial x_j}$, that is ∇ is dotted with the rows of $\overline{u_i u_j}$, and $R_{ij} = \overline{u \otimes u}$ is the Reynolds stress, see [4]. The Reynolds stress has the interpretation of a turbulent momentum flux and the last term in (4) is also know as the eddy viscosity. It describes how the small scales influence the large scales. In addition we get divergence free conditions for U, and u

$$\nabla \cdot U = 0, \qquad \nabla \cdot u = 0.$$

Together, (4) and the divergence free condition on U give the Reynolds Averaged Navier-Stokes (RANS) that forms the basis for most contemporary simulations of turbulent flow. The large scale equation (4) is satisfied by the mean flow $U =$ constant, in the measurement region of the VDTT. Thus in our case (4) reduces to the pressure gradient balancing the eddy viscosity.

Finding a constitutive law for the Reynolds stress $\overline{u \otimes u}$ is the famous closure problem in turbulence and we will solve that by writing down a stochastic equation for the small scale velocity u. This was first done by Landau and Lifschitz in [15].

The consequence of the SCT hypothesis is that the fluctuating velocity u in turbulence is a stochastic process that is determined by a stochastic partial differential equation (SPDE). It will be the Navier-Stokes equation for the fluctuations driven by noise, see below. This is the point of view taken by Kolmogorov in [13, 12, 14], but the question we have to answer is: what is the form of the noise? There is a large literature on this question, trying to trace the form of the noise back to the fluid instabilities, but these attempts have proven to be unsuccessful. Any memory of the fluid instabilities is quickly forgotten in fully-developed turbulence and the noise seems to be of a general form. Thus it makes sense to try to put generic noise into the Navier-Stokes equations and see how the Navier-Stokes evolution colors generic noise. Below we will answer what generic noise in the Navier-Stokes equation must look like, see [6] for more details.

For fully developed turbulence, we close the model with a stochastic forcing term to account for the small scales in (2). This noise term models the dissipation in the flow. We impose periodic boundary conditions and assume the dissipation processes in the flow are weakly coupled. Then, applying the Functional Central Limit Theorem to the dissipation processes gives the mean of these processes as

$$\bar{D} = \sum_{k \neq 0} c_k^{\frac{1}{2}} db_t^k e_k(x),$$

where $e_k(x) = e^{2\pi i k x}$ are distinct Fourier compoents complete with its own Brownian motion b_t^k, and $c_k^{\frac{1}{2}}$ are coefficients that converge sufficiently fast enough to

ensure convergence of the entire series, see [6]. However, there are fluctuations in the mean of the dissipation which, through an application of the Large Deviation Principle to the dissipation processes, yield the term

$$D' = \sum_{k\neq 0} d_k |k|^{\frac{1}{3}} dt e_k(x).$$

Here, $e_k(x)$ is defined as above and d_k is defined similarly to $c_k^{\frac{1}{2}}$. These two terms defined the additive noise forcing term. A detailed description of these terms is given in [6]. A final forcing term comes from the multiplicative noise. This models jumps in the velocity gradient or vorticity concentrations. If we let N_t^k denote the number of velocity jumps associated to the k-th wave number that have occured by time t. This in turn implies that the differential

$$dN^k(t) = N^k(t+dt) - N^k(t)$$

denotes the number of jumps in the time interval $(t, t+dt]$. Then the multiplicative noise has the form

$$J = \sum_{k\neq 0} \int_{\mathbb{R}} h_k(t,z) \bar{N}^k(dt,dz),$$

where h_k measures the size of the jump and $\bar{N}^k$ is the compensated number of jumps. Hence, adding the terms $\bar{D}$, D' and, J multiplied by u, to the Navier-Stokes equation, we get a stochastic PDE describing the fully developed turbulent small-scale flow in the wind tunnel:

$$\begin{aligned} du + u\cdot\nabla u dt = {} & [\nu\Delta u + \nabla(\Delta^{-1}[\mathrm{Trace}(\nabla u)]) - u\cdot\nabla U - U\cdot\nabla u]dt \\ & + \sum_{k\neq 0} d_k |k|^{\frac{1}{3}} dt e_k(x) + \sum_{k\neq 0} c_k^{\frac{1}{2}} db_t^k e_k(x) \\ & + u \sum_{k\neq 0} \int_{\mathbb{R}} h_k(t,z) \bar{N}^k(dt,dz). \end{aligned} \tag{5}$$

In integral form, the stochastic Navier Stokes equation governing fully developed turbulence is given by

$$\begin{aligned} u = {} & e^{K(t)} e^{\int_0^t dq} M_t u^0 + \sum_{k\neq 0} c_k^{\frac{1}{2}} \int_0^t e^{K(t-s)} e^{\int_s^t dq} M_{t-s} db_s^k e_k(x) \\ & + \sum_{k\neq 0} d_k \int_0^t e^{K(t-s)} e^{\int_s^t dq} M_{t-s} |k|^{\frac{1}{3}} dt e_k(x), \end{aligned} \tag{6}$$

where K is the operator

$$K = \nu\Delta + \nabla\Delta^{-1}\text{Trace}(\nabla u \nabla), \tag{7}$$

M_t is the exponential martingale, see below, $e_k(x) = e^{2\pi ikx}$ is a Fourier component complete with its own Brownian motion b_t^k, and the coefficients $c_k^{\frac{1}{2}}$ and d_k decay fast enough so that the series converges, see [6], Chapter 1. We drop the term $-u \cdot \nabla U$, in the equation above, since the mean flow U is approximately constant in the VDTT, see [8]. Thus, we have that

$$u(x,t) - u(y,t) = \tag{8}$$
$$\sum_{k\neq 0}\left[(c_k^{\frac{1}{2}}\int_0^t e^{K(t-s)}e^{\int_s^t dq}M_{t-s}db_s^k + d_k\int_0^t e^{K(t-s)}e^{\int_s^t dq}M_{t-s}|k|^{\frac{1}{3}}ds)(e_k(x)-e_k(y))\right],$$

where $u(x,t)$ and $u(y,t)$ are the flow velocities at two points x and y in the wind tunnel. This permits us to describe the computation of the structure functions:

$$S_p(x-y,t) = E(|u(x,t)-u(y,t)|^p).$$

First, we note that the expectation is actually a composition of two expectations, one for the Brownian motion, denoted E_b and the other for the log-Poisson process, denoted E_p. The log-Poisson expectation acts upon the term

$$e^{\int_s^t dq} = \exp\{\frac{\frac{2}{3}\ln|k| + N_k\ln(\frac{2}{3})}{3}\} = (|k|^{\frac{2}{3}}(\frac{2}{3})^{N_t^k})^{\frac{1}{3}},$$

given by the Feynman-Kac formula, see [6]. Then, we get that

$$E_p([|k|^{\frac{2}{3}}(\frac{2}{3})^{N_t^k}]^{\frac{p}{3}}) = |k|^{-(-\frac{2p}{9}+2(1-(\frac{2}{3})^{\frac{p}{3}}))},$$

see [6]. Notice the exponent above is the She-Leveque intermittency correction (1), denoted τ_p. Applying E_p also eliminates all terms $(e_k(x)-e_k(y))(e_j(x)-e_j(y))$ for $k \neq j$. Standard algebra and trigonometry gives

$$e_k(x) - e_k(y) = 2e^{\pi ik(x+y)}\sin(\pi k\cdot(x-y)).$$

Thus, we get that

$$E(|u(x,t)-u(y,t)|^p) = \tag{9}$$

$$E(\Big|\sum_{k\neq 0}\Big[(c_k^{\frac{1}{2}}\int_0^t e^{K(t-s)}e^{\int_s^t dq}M_{t-s}db_s^k + d_k\int_0^t e^{K(t-s)}e^{\int_s^t dq}M_{t-s}|k|^{\frac{1}{3}}ds)(e_k(x)-e_k(y))\Big]\Big|^p)$$

$$= E_b(\Big|\sum_{k\neq 0}\Big[(c_k^{\frac{1}{2}}\int_0^t e^{K(t-s)}|k|^{-\tau_p}M_{t-s}db_s^k) + d_k\int_0^t e^{K(t-s)}|k|^{-\tau_p}M_{t-s}|k|^{\frac{1}{3}}ds)\Big]$$

$$\times 2e^{\pi ki(x+y)}\sin(\pi k\cdot(x-y))\Big|^p).$$

Now, we use a eigenvalue estimate for the operator $-K$, replacing it with $\lambda_k = C|k|^{\frac{2}{3}} + 4\nu\pi^2|k|^2$, see [6]. This estimate assumes ergodicity and that the expectation of the norm of u in the Sobolev space $H^{\frac{11}{6}^+}$ is finite, see Lemma 2.7 in [6]. We will discuss this in more detail below. M_t is the exponential martingale:

$$M_t = \mathrm{Exp}[\int (U+u)\cdot dB_s - \int \frac{|U+u|^2}{2}ds],$$

where $B_t \in \mathbb{R}^3$ is an auxiliary Brownian motion and $U+u$ is the Reynolds decomposition of the flow. A simple application of Ito's formula yields

$$M_t^p = 1 + \int_0^t (U+u)M_s\cdot dB_s + \frac{p(p-1)}{2}\int_0^t |U+u|^2 M_s^p ds.$$

Thus, we have

$$\begin{aligned} E[M_t^p] &= 1 + \frac{p(p-1)}{2}\int_0^t E[|U+u|^2 M_s^p]ds \\ &\leq 1 + \frac{p(p-1)}{2}\int_0^t E[|U+u|^4]^{1/2}E[M_s^{2p}]^{1/2}ds \end{aligned}$$

by the Cauchy-Schwarz inequality. A consideration of the fourth structure function below shows that last term only contributes higher order (in k) terms to the denominator of the structure functions. We will ignore this small correction term below.

Finally, we take the absolute value and expand the polynomial expression in (9). To ultimately compute the structure functions, we use Ito's Lemma

$$E[(\int_S^T f(t,w)dB_t)^2] = \int_S^T E[(f(t,w))^2]dt$$

to turn any even power of the stochastic integral into a deterministic integral, which can then be solved for using standard calculus. For odd powers, we use the fact that

$$E[\int_S^T f dB_t] = 0$$

to eliminate such terms. We then find the first structure function is given by

$$\begin{aligned} E(|u(x,t)-u(y,t)|) &= S_1(x,y,t) \\ &= \frac{2}{C}\sum_{k\in\mathbb{Z}^3\setminus\{0\}} \frac{|d_k|(1-e^{-\lambda_k t})}{|k|^{\zeta_1}+\frac{4\pi^2\nu}{C}|k|^{\zeta_1+\frac{4}{3}}}|\sin(\pi k\cdot(x-y))|, \end{aligned} \tag{10}$$

where $|\cdot|$ denotes the vector norm in $\mathbb{R}^3$. The second structure function is given by

$$\begin{aligned} E(|u(x,t)-u(y,t)|^2) &= S_2(x,y,t) \\ &= \frac{4}{C^2}\sum_{k\in\mathbb{Z}^3}\Big[(|\sin^2(\pi k\cdot(x-y))|) \\ &\Big\{\frac{\frac{C}{2}c_k(1-e^{-2\lambda_k t})}{|k|^{\zeta_2}+\frac{4\pi^2\nu}{C}|k|^{\zeta_2+\frac{4}{3}}} \\ &+\frac{|d_k|^2(1-e^{-\lambda_k t})}{|k|^{\zeta_2}+\frac{8\pi^2\nu}{C}|k|^{\zeta_2+\frac{4}{3}}+\frac{16\pi^4\nu^2}{C^2}|k|^{\zeta_2+\frac{8}{3}}}\Big\}\Big] \end{aligned} \tag{11}$$

where $c_k = |c_k^{\frac{1}{2}}|^2$. The third structure function is given by

$$\begin{aligned} E(|u(x,t)-u(y,t)|^3) &= S_3(x,y,t) \\ &= \frac{8}{C^3}\sum_{k\in\mathbb{Z}^3}\Big[(|\sin^3(\pi k\cdot(x-y))|) \\ &\Big\{\frac{\frac{C}{2}c_k|d_k|(1-e^{-2\lambda_k t})(1-e^{-\lambda_k t})}{|k|^{\zeta_3}+\frac{8\pi^2\nu}{C}|k|^{\zeta_3+\frac{4}{3}}+\frac{16\pi^4\nu^2}{C^2}|k|^{\zeta_3+\frac{8}{3}}} \\ &+\frac{|d_k|^3(1-e^{-\lambda_k t})^3}{|k|^{\zeta_3}+\frac{12\pi^2\nu}{C}|k|^{\zeta_3+\frac{4}{3}}+\frac{48\pi^4\nu^2}{C^2}|k|^{\zeta_3+\frac{8}{3}}+\frac{64\pi^6\nu^3}{C^3}|k|^{\zeta_3+4}}\Big\}\Big] \end{aligned} \tag{12}$$

The general p-th structure function is given by

$$S_p(x,y,t) = \frac{2^p}{C^p}\sum_{k\neq 0} A_p \times |\sin^p[\pi k\cdot(x-y)]|, \tag{13}$$

where

$$A_p = \frac{2^{\frac{p}{2}}\Gamma(\frac{p+1}{2})\sigma_k^p {}_1F_1(-\frac{1}{2}p, \frac{1}{2}, -\frac{1}{2}(\frac{M_k}{\sigma_k})^2)}{|k|^{\zeta_p} + \frac{p_k\pi^2\nu}{C}|k|^{\zeta_p+\frac{4}{3}} + O(\nu^2)}, \tag{14}$$

where Γ is the gamma function, ${}_1F_1$ is the hypergeometric function, $M_k = |d_k|(1 - e^{-\lambda_k t})$, $\sigma_k = \sqrt{(\frac{C}{2}c_k(1-e^{-2\lambda_k t}))}$, and p_k is different for each denominator term in the series. Note that the Reynolds number dependence is captured via the viscosity term ν. C is a constant approximating the mean velocity of the flow. It will allowed to vary across structure functions to accommodate a relative change in the mean and the large deviations.

4 The One-dimensional Structure Functions

We want to fit the structure functions (13) to the experimental data collected in the VDTT, but to do this we have to reduces the three-dimensional structure functions to one-dimensional ones. One can consider structure functions where the measurements are take at two distinct points along the length of the tunnel, in the direction of the mean velocity. These are called the longitudinal structure functions, $S_p(r,t)$, where $r = x - y$, is a vector along the main axis of the tunnel. Or, one can consider the transversal structure functions, $S_p(q,t)$, where $q = x - y$, is a vector in the radial direction of the tunnel, perpendicular to r. In homogeneous turbulence these two structure functions are not independent. In fact, one can show, see [18], that the correlation matrix is given by

$$D_{ij} = E[(u_i(x,t) - u_i(y,t))(u_j(x,t) - u_j(y,t))] = S_2(r,t)I + (S_2(r,t) - S_2(q,t))\frac{r_i r_j}{r^2},$$

where I is the identity matrix in $\mathbb{R}^3 \times \mathbb{R}^3$, and

$$S_2(q,t) = S_2(r,t) + r\frac{\partial}{\partial r}S_2(r,t),$$

with $r = |r|$, $|\cdot|$ denoting the vector norm in $\mathbb{R}^3$. For $\eta << r$, D_{ij} is expected to reduce to

$$D_{ij} = C_2(\varepsilon r)^{2/3}(\frac{4}{3}I - \frac{1}{3}\frac{r_i r_j}{r^2}).$$

Thus in $\mathbb{R}^3$ the correlation matrix is determined by longitudinal structure function alone and we will restrict our attention to them.

Consider the longitudinal third structure function above,

$$S_3(r,t) = \frac{8}{C^3}\sum_{k\in\mathbb{Z}^3}\Big[(|\sin^3(\pi k\cdot r)|)\Big\{\frac{\frac{C}{2}c_k|d_k|(1-e^{-2\lambda_k t})(1-e^{-\lambda_k t})}{|k|^{\zeta_3}+\frac{8\pi^2\nu}{C}|k|^{\zeta_3+\frac{4}{3}}+\frac{16\pi^4\nu^2}{C^2}|k|^{\zeta_3+\frac{8}{3}}} + \frac{|d_k|^3(1-e^{-\lambda_k t})^3}{|k|^{\zeta_3}+\frac{12\pi^2\nu}{C}|k|^{\zeta_3+\frac{4}{3}}+\frac{48\pi^4\nu^2}{C^2}|k|^{\zeta_3+\frac{8}{3}}+\frac{64\pi^6\nu^3}{C^3}|k|^{\zeta_3+4}}\Big\}\Big],$$

where $c_k = c_1+c_2+c_2$, $|d_k| = \sqrt{d_1^2+d_2^2+d_2^2}$ and $|k| = \sqrt{k_1^2+k_2^2+k_2^2}$, and $r = x-y$. If we take $r=(r,0,0)$ to lie along the axis of the VDTT (cylinder), then $r\cdot k = (rk_1,0,0)$ and if we ignore k_2 and k_3 in the denominator of S_2, and take $t\to\infty$, we get the inequality

$$S_3(r,t) \le \frac{8}{C^3}\sum_{k_1\neq 0}\Big[(|\sin^3(\pi k_1 r)|)\Big\{\frac{\frac{C}{2}\tilde{c}_{k_1}|\tilde{d}_{k_1}|}{|k_1|^{\zeta_3}+\frac{8\pi^2\nu}{C}|k_1|^{\zeta_3+\frac{4}{3}}+\frac{16\pi^4\nu^2}{C^2}|k_1|^{\zeta_3+\frac{8}{3}}} + \frac{|\tilde{d}_{k_1}|^3}{|k_1|^{\zeta_3}+\frac{12\pi^2\nu}{C}|k_1|^{\zeta_3+\frac{4}{3}}+\frac{48\pi^4\nu^2}{C^2}|k_1|^{\zeta_3+\frac{8}{3}}+\frac{64\pi^6\nu^3}{C^3}|k_1|^{\zeta_3+4}}\Big\}\Big],$$

because $\zeta_3 = 1$, where $\tilde{c}_{k_1} = \sum_{k_2\neq 0}\sum_{k_3\neq 0} c_{(k_1,k_2,k_3)}$, $|\tilde{d}_{k_1}| = \sum_{k_2\neq 0}\sum_{k_3\neq 0}|d_{(k_1,k_2,k_3)}|$. We have used the convexity of the functions $f(x) = x^p,\ p\ge 1$ to take the sum into the powers, here $p = 1,3$. This upper estimate, that is supposed to be close, reduces the three dimensional S_3 to the one dimensional one. The argument for all the structure functions $S_p,\ p\ge 3$, is similar but the argument does not hold for $p = 1$, or 2, because $\zeta_1 = 0.37$ and $\zeta_2 = 0.696$ so both are less than one. This means that the upper estimate does not hold for all $|k|$s, only the ones that are big enough so that the second term in the denominators of S_1 and S_2 dominates the first. We will use the upper estimate with this understanding. We will compare the one dimensional structure function with experimental data and drop the subscript 1 on k_1. Thus the general p-th one-dimensional longitudinal structure function, in the stationary state, is given by

$$S_p(r,t) \le \frac{2^p}{C^p}\sum_{k\neq 0}\frac{2^{\frac{p}{2}}\Gamma(\frac{p+1}{2})\sigma_k^p\,{}_1F_1(-\frac{1}{2}p,\frac{1}{2},-\frac{1}{2}(\frac{M_k}{\sigma_k})^2)}{|k|^{\zeta_p}+\frac{p_k\pi^2\nu}{C}|k|^{\zeta_p+\frac{4}{3}}+O(\nu^2)}|\sin^p[\pi kr]|, \qquad (15)$$

where Γ is the gamma function, ${}_1F_1$ is the hypergeometric function, $M_k = |\tilde{d}_k|$, $\sigma_k^2 = \frac{C}{2}\tilde{c}_k$, and p_k is different for each denominator term in the series. Note that

the Taylor-Reynolds number dependence is captured via the viscosity term ν. C is a constant approximating the mean velocity of the flow. The upper estimate is understood to hold for $p = 1,2$ when $|k|$ is large enough.

We can think about the triple sum as an integral

$$\sum_{k\in\mathbb{Z}^3\setminus\{0\}} c_k \sim \int_0^\infty \int_\omega c_k d\omega |k|^2 d|k| = \int_0^\infty \tilde{c}_k dk \sim \sum_{k\neq 0} \tilde{c}_k,$$

where $|k|$ is the radius of the three-vector k. This means that

$$\tilde{c}_k = \int_\omega c_k d\omega |k|^2,$$

is the integral of c_k over a sphere of radius k is Fourier space, analogous to the energy shell in the Kolmogorov-Obukhov cascade. Thus, whereas $c_k \sim \frac{1}{k^{3+\varepsilon}}$, where $k = |k|$, in order for the sum to converge, $\tilde{c}_k \sim \frac{1}{k^{1+\varepsilon}}$. A similar argument applies to $\sum_{k\in\mathbb{Z}^3\setminus\{0\}} |d_k|$ For this reason we expect the exponent m of k below to satisfy $m > 1$. We will in fact make the ansatz,

$$\tilde{c}_k = \sqrt{\frac{2}{\pi}} \frac{b}{b^2 + k^m},\ \tilde{d}_k = \sqrt{\frac{2}{\pi}} \frac{a}{a^2 + k^m}, \tag{16}$$

where $\tilde{c}_k$ and $\tilde{d}_k$ are the one-dimensional versions of the coefficients in the structure functions, to approximate the experimental data. Provided that m is greater than 1, the series determining the one dimensional restriction of the structure functions (15) will converge. The $\sqrt{\frac{2}{\pi}}$ factor in both formulas is placed there to compensate for the Fourier Transform operation in Mathematica. The thinking here is that there is a universal coefficient m for each Reynolds number that will determine how fast the sine series converges, and thus the spatial smoothness of the structure functions. Thus for k large, $\tilde{c}_k$ and $\tilde{d}_k \sim \frac{1}{k^m}$. Moreover, we are (optimistically) assuming that the two contributions $\tilde{c}_k$ and $\tilde{d}_k$, to the large eddies, also scale with the order of the structure functions and can be characterized by a number b, respectively a, for each Taylor-Reynolds number. Thus for k small, $\tilde{c}_k \sim \frac{1}{b}$ and $\tilde{d}_k \sim \frac{1}{a}$. This turns out to work reasonably well, see Table 5.

In conclusion, we are able to reduce the three-dimensional coefficients c_k and d_k to the one-dimensional coefficients $\tilde{c}_k$ and $\tilde{d}_k$, respectively, and so use the one-dimensional formulas to fit to the data, and formulate a simple ansatz (16), for coefficient's dependance on the Taylor-Reynolds number and the wavenumber $1/k$.

5 Comparison of the Model with the Data

The data in this paper comes from the Max Planck Institute for Dynamical and Self-Orgranization, located in Göttingen, Germany and was generated by the Variable Density Turbulence Tunnel (VDTT). The pressurized gases circulate in the VDTT in an upright, closed loop. At the upstream end of two test sections, the free stream is disturbed mechanically. The data in the current paper is generated by a fixed grid but the gas stream can also be disturbed by an active grid resulting in even higher Reynolds number turbulence. In the wake of the grid the resulting turbulence evolves down the length of the tunnel without the middle region being substantially influenced by the walls of the tunnel, see [8]. The measurements were performed with a Dantec StreamLine hot wire anemometry system, see [8].

The measurements were taken at a distance 7.1 meter downstream from a 186.6 mm classical grid, on a array of 150 points covering a 60×60 cm^2 square centered in the cross section of the tunnel. The longitudinal differences are

$$\delta u(x,r) = u(y,t) - u(x,t) = u(x+r,t) - u(x,t)$$

where u, x and r are parallel vectors (along the x-axis). Taylor's frozen flow hypothesis is used to extract x and r from the time series of the probe, see [8]. The test sections are about 8 meters long, long enough for the turbulence to evolve through at least one eddy turnover time, around 1 second, see [8]. This means that the turbulence can be observed over the time that it takes the energy to cascade all the way from the large eddies to the dissipate scale. More details about the tunnel can be found in [8].

Measurements were taken for Taylor Reynolds Numbers 110, 264, 508, 1000, and 1450. The pertinent parameters for the data are given Table 1. The system length in the tunnel is an important value for fitting the data because we have to scale the lag variable r, $\frac{r/\eta}{\text{system length}} = (x-y)$, with the system length. One might think that the system length is the square root of the cross sectional value of the tunnel $\sqrt{A}$, but in fact the relevant system length is the grid size of the grid used to perturb the gas flow upstream from the measurement section. This raises the question whether the grid size influences the shape of the largest eddies in the flow and we will see below that the answer is yes, it does so for the smaller Reynolds numbers. For the larger Reynolds numbers this influence disappears, see Table 5.

The structure function were plotted against $\frac{r}{\eta}$, where r is the distance between positions x and y as given by the Taylor Frozen Flow Hypothesis and η is the Kolmogorov length scale. The final recorded data point occurs at $\frac{r}{\eta} = 19540$.

Taylor Reynolds Number	η	L	ν
110	1025	165.1	0.0000155
264	162	102.5	0.00000234
508	91	123.9	0.000001
1000	36	136.6	0.000000291
1450	22	129.5	0.00000015

Table 1: Here, η is the Kolmogorv length scale given in micrometers, L is the Taylor length scale given in millimeters, and ν is the viscosity given in $\frac{m^2}{s}$.

Thus, we substitute $\frac{r}{\eta}/(19540(D))$ for $x-y$, where D is an constant greater than 1, in the above formulas. This is done to compensate for the system length of each measurement. We assume periodic boundary conditions in the Navier Stokes equation (2) and (5). Thus, we divide $\frac{r}{\eta}$ by $19540(D)$ so that our sine series formula will capture the entire data set. Once found, the system length is fixed for a particular Taylor Reynolds number across the varying structure functions. The found values for D are given in Table 5.

Fitting was done in Mathematica using the internal FindFit command. Due to computational time, the series given in Section 4 was run out to one thousand terms. Initial fitting to the formulas given in Section 4 proved to not be effective. It was assumed that the largest eddies were influenced by the active grid in the wind tunnel and thus, were influencing the fitting routine. Thus, to compensate, the first two sine terms were allowed to have free coefficients. In other words, the new model used to fit the data is given by

$$A_1|\sin[(\pi\times r)/(19540.3(D))]|+A_2|\sin^2[(2\pi\times r)/(19540.3(D))]| + \sum_{k=3}\frac{2^p}{C^p}A_p|\sin^p[\pi k\cdot(x-y)]|, \tag{17}$$

where A_p is still given by (15) This was done for all structure function fits. Experimentation found that the best result came from using the fourth structure function for each Taylor Reynolds Number to fix the coefficients a, b, and D. This is likely the result of the Fourth Structure Function being the largest structure function still bound by the Sobolev inequality, see Section 9.

Tables 2, 3, and 4 contain the found values for A_1, A_2 and C respectively, as described in (17).

Re Lambda	110	264	508	1000	1450
Second	0.00744	.0153	.0169	.0183	.0195
Third	.00154	.00162	.00484	.00564	.00664
Fourth	.000384	.00189	.00228	.00251	.00305
Sixth	.0000341	.000431	.000566	.000552	.000691
Eighth	$3.12(10^{-6})$	.0000839	.000122	.000144	.000204

Table 2: The fitted values for A_1 in equation (17).

Re Lambda	110	264	508	1000	1450
Second	.00285	.00583	.00653	.00697	.00666
Third	.000872	.00124	.00526	.00488	.00395
Fourth	.000174	.000746	.000804	.001	.0006
Sixth	$4.24(10^{-6})$	-.0000756	-.00011	.0000919	.0000654
Eighth	$1.04(10^{-6})$	.0000127	.0000147	.0000264	$-4.71(10^{-7})$

Table 3: The fitted values for A_2 in equation (17).

Taylor Reynolds Number	110	264	508	1000	1450
Second	2.8	3.31	4.21	7.62	21.1
Third	1.4	1.93	1.49	2.72	3.59
Fourth	1.07	1.01	1.19	2.36	6
Sixth	1.15	1.29	1.34	1.73	2.49
Eighth	0.616	.531	.596	1.17	2.84

Table 4: The fitted values for C in eq. (17)

Taylor Reynolds Number	a	b	D
110	11.64	0.01612	1.569
264	9.581	0.05236	1.769
508	8.314	0.06504	1.518
1000	3.792	0.09247	1.32
1450	2.684	0.4092	1.3

Table 5: The fitted values for a, b, and D in eq. (15)

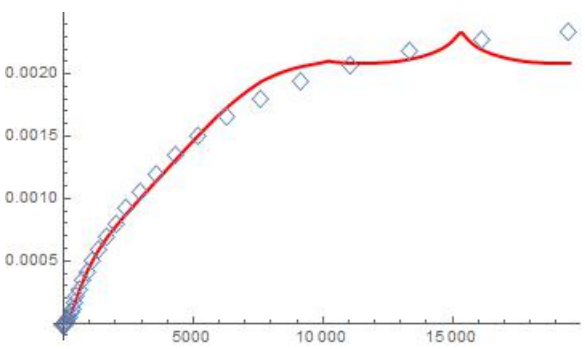

(a) Third Structure Function, Normal Scale

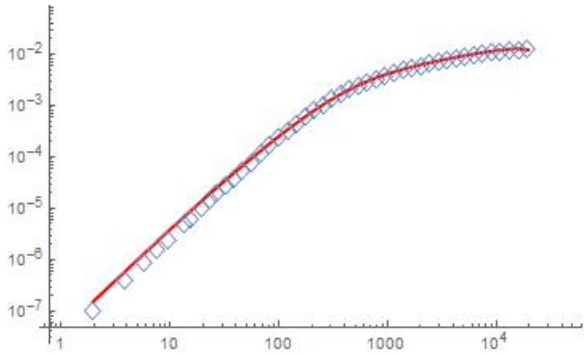

(b) Second Structure Function

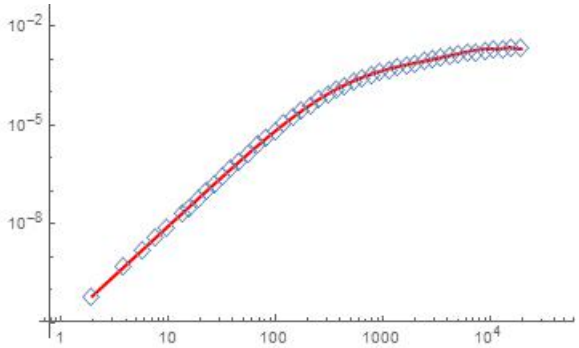

(c) Third Structure Function

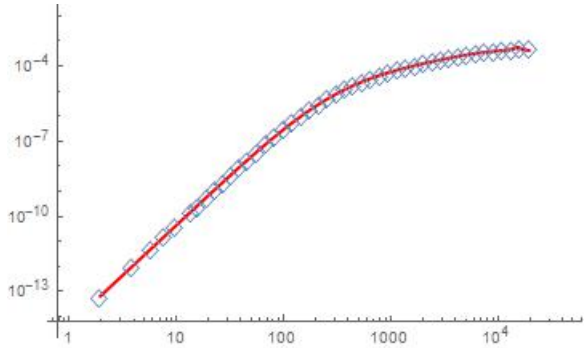

(d) Fourth StructureFunction

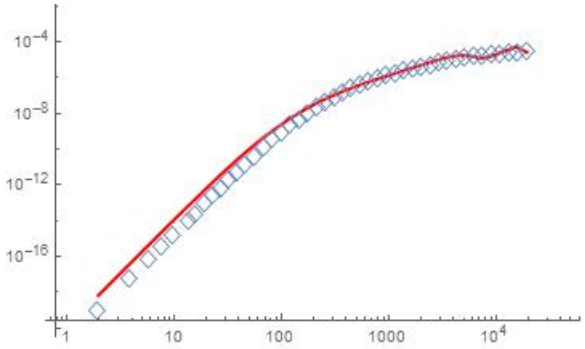

(e) Sixth Structure Function

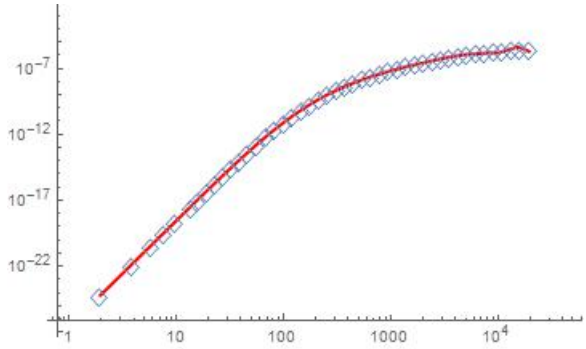

(f) Eighth Structure Function

Figure 1: Taylor Reynolds Number 110. Note that the plots (b)-(f) are made on a log-log scale.

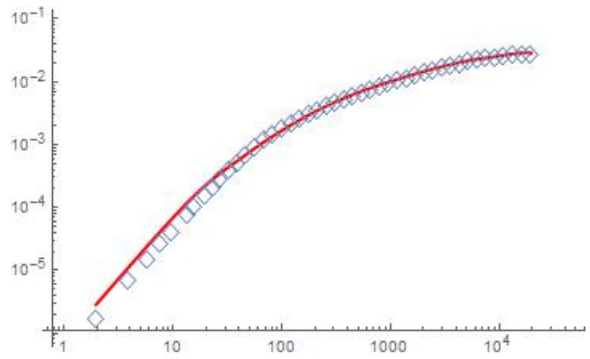

(a) Second Structure Function

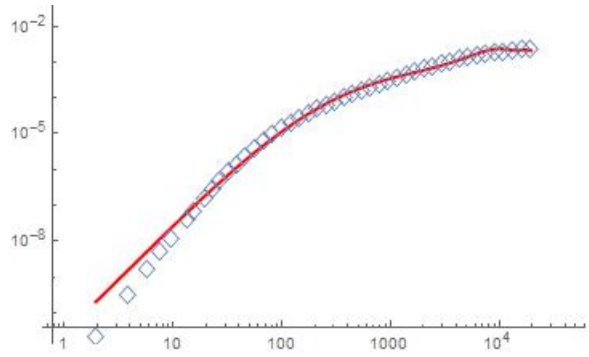

(b) Third Structure Function

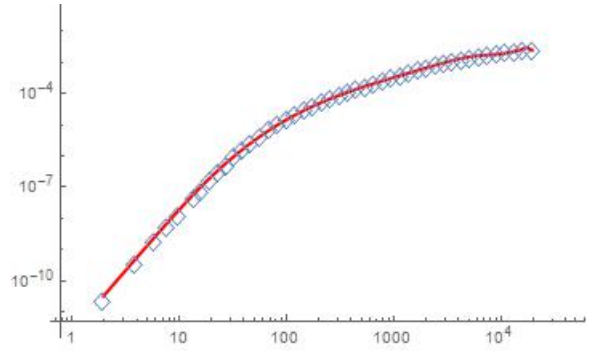

(c) Fourth StructureFunction

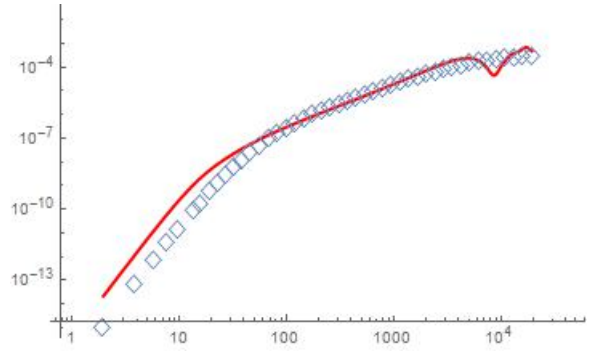

(d) Sixth Structure Function

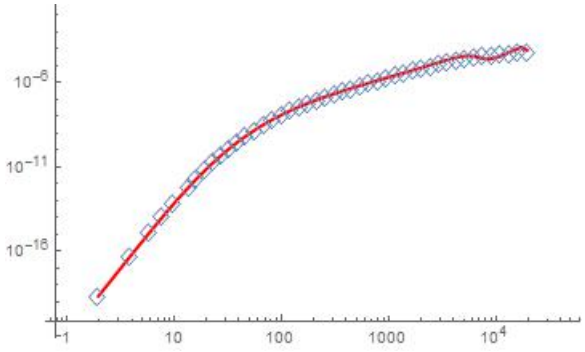

(e) Eighth Structure Function

Figure 2: Taylor Reynolds Number 264. Note that the plots are made on a log-log scale.

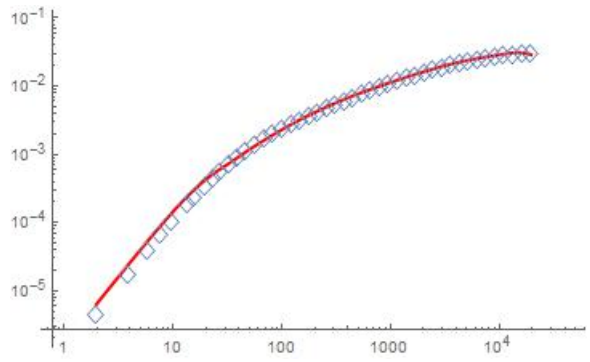

(a) Second Structure Function

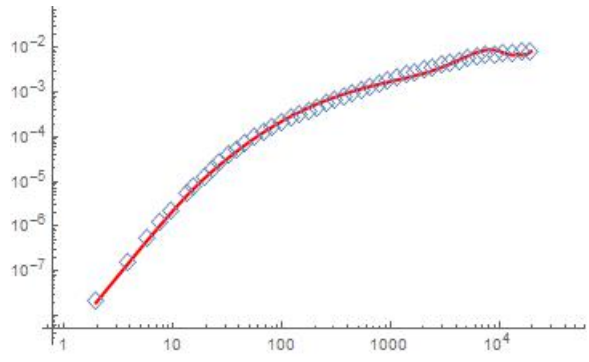

(b) Third Structure Function

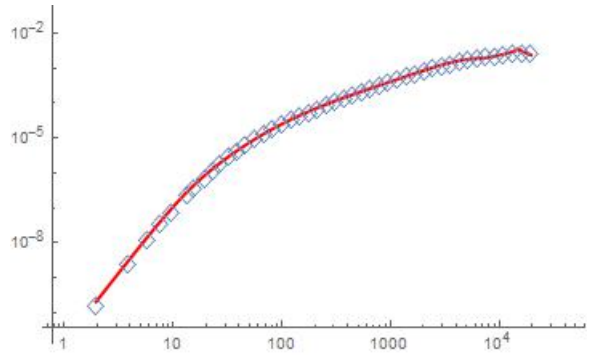

(c) Fourth StructureFunction

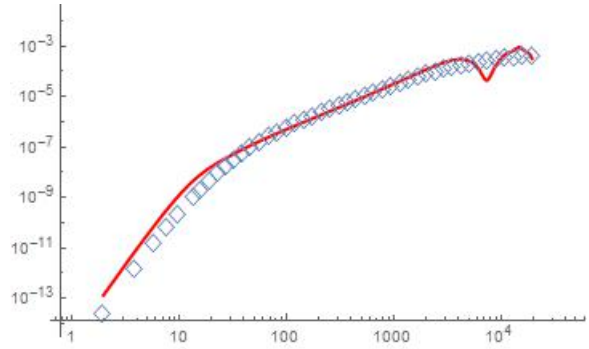

(d) Sixth Structure Function

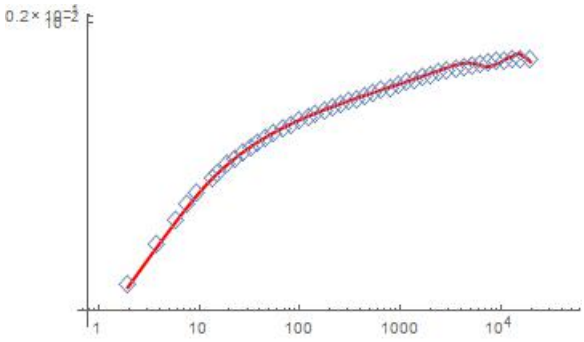

(e) Eighth Structure Function

Figure 3: Taylor Reynolds Number 508. Note that the plots are made on a log-log scale.

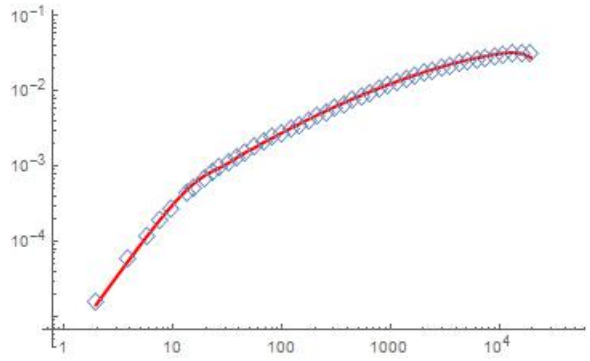

(a) Second Structure Function

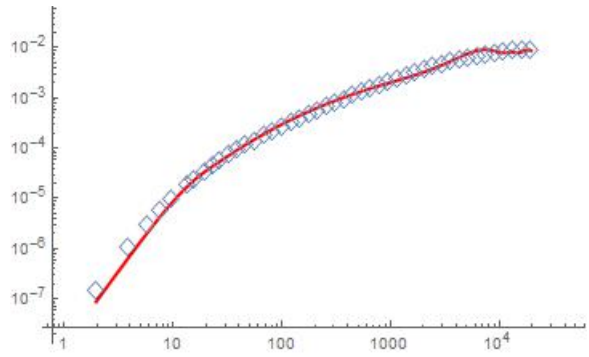

(b) Third Structure Function

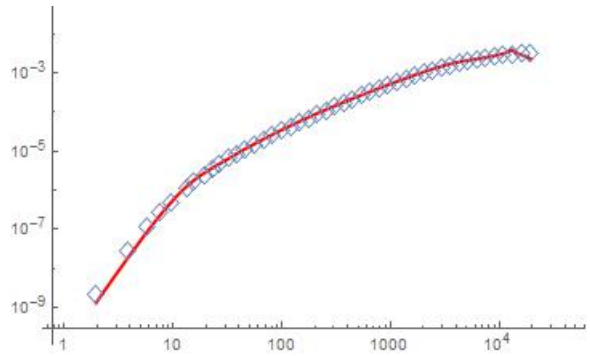

(c) Fourth StructureFunction

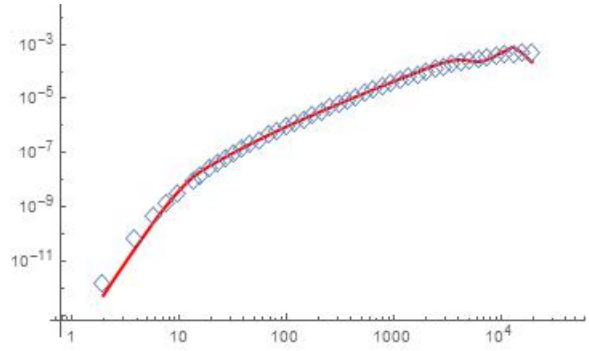

(d) Sixth Structure Function

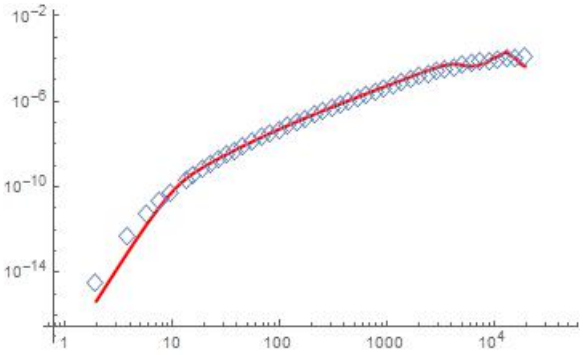

(e) Eighth Structure Function

Figure 4: Taylor Reynolds Number 1000. Note that the plots are made on a log-log scale.

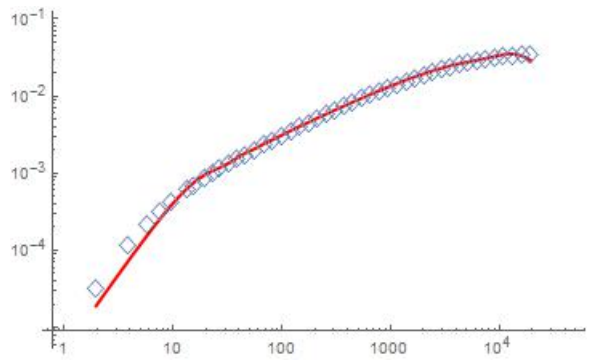

(a) Second Structure Function

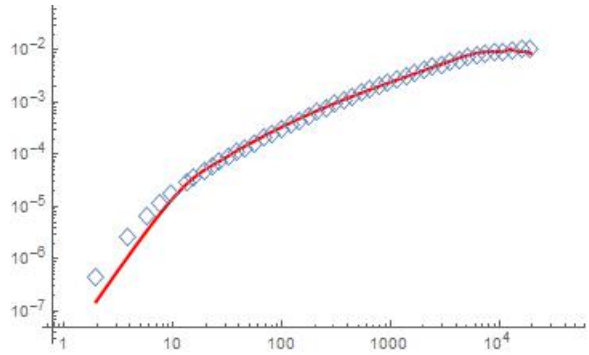

(b) Third Structure Function

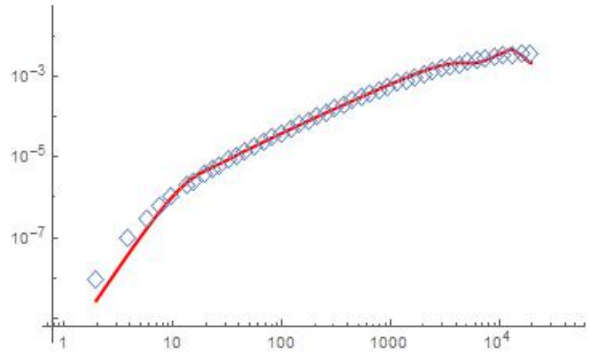

(c) Fourth StructureFunction

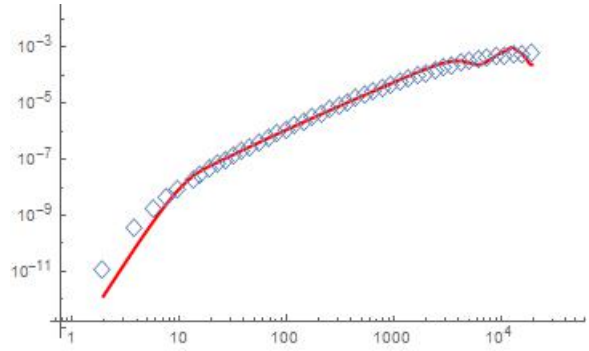

(d) Sixth Structure Function

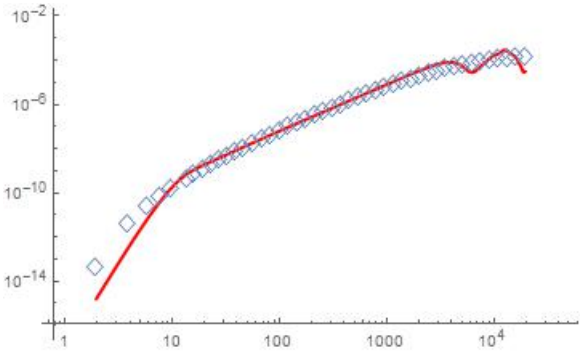

(e) Eighth Structure Function

Figure 5: Taylor Reynolds Number 1450. Note that the plots are made on a log-log scale.

Taylor Reynolds Number	110	264	508	1000	1450
Second	1.563	1.16	1.069	.8965	.9148
Third	1.408	1.185	0.922	.6488	.5262
Fourth	1.269	.8751	.7936	.5554	.4865
Sixth	.98607	.5055	.5192	.4339	.3398
Eighth	.9711	.5924	.5755	.3771	.2482

Table 6: The fitted values for m in eq. (15)

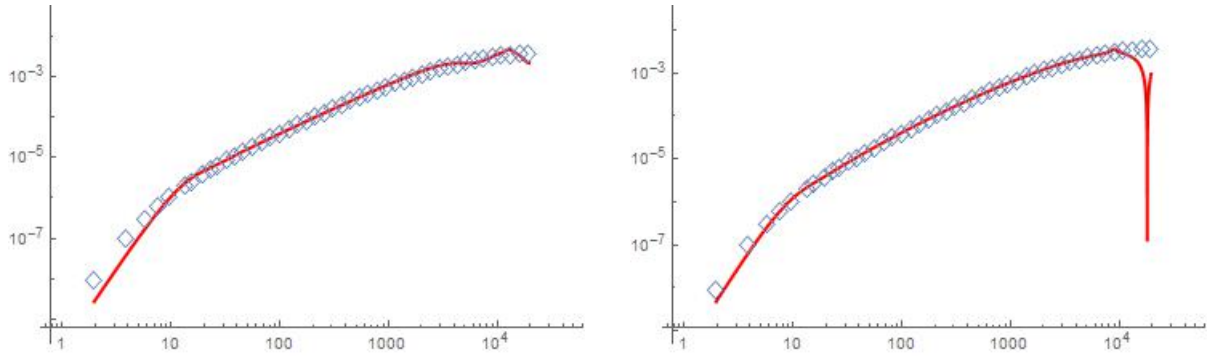

(a) Fourth Structure Function as shown in figure 5 (b) Fourth Structure Function at $D = 0.920864$

Figure 6: The two different fits for Taylor Reynolds number 1450.

6 Evaluation of the Model

Below are the fitting results for the data. The blue diamonds are the data points while the red line is our fitted function. All the plots are on a log-log scale except for a single plot of the third structure function at Taylor Reynolds Number 110. This is included for perspective. We see that the fitting is good for most of the structure function for most of the Reynolds numbers. There are little wiggles at the largest scales (largest values of the lag variable). This is presumably related to the interaction between the turbulence and the grid and the grids influence on the largest eddies as discussed above. At the highest Reynolds numbers and highest order (sixth and eighth) structure functions, we see a divergence at the smallest scales (smallest values of the lag variable). This is indicative of the divergence of the series for these structure functions at the highest Reynolds numbers. In general, we note that the fits become less accurate as we increase the structure function number. The fits for the second, third, and fourth structure functions are generally quite good but the sixth and eighth structure function fits are rougher. This is expected from the theory given by in [6], see below.

Table 5 gives the fitted values for a and b. This table shows that the Central Limit Theorem term as given by b has a greater influence for smaller Taylor Reynolds numbers than the Large Deviation Principle term, as given by a, as for small values of k, these terms essentially become $\frac{1}{a}$ and $\frac{1}{b}$, respectively. As the Reynolds number goes up, we do see a decreasing influence of b and an increasing influence of a, although b still remains the more influential parameter. Thus the contribution of the Central Limit Theorem is greater. The influence of the grid on the lowest Fourier modes A_1 and A_2 is plotted in Tables 2 and 3. These contributions are small for low order structure functions and become insignificant for the higher order structure functions, for all Reynolds numbers. Thus the influence of the grid on large eddies is small and becomes negligible for the higher structure functions.

The values of the exponent m of the wavenumber $k = k_1$ are given in Table 6. In general the exponents are larger or very close to 1, towards the top of the table. The first (top) line in Table 6, corresponding to the second structure function, verifies the hypothesis on the coefficients c_k and d_k in Sections 2 and 4. The energy shell coefficient $\tilde{c}_k$ and $\tilde{d}_k$ should decay as $|k|^{-m}$, $m > 1$. All the exponents in the first line in Table 6 satisfy this except the last two. However, both still lie within the fitting uncertainty and may be explained by the Reynolds number corrections absorbing the weight of the power. Thus the exponents $m(R_\lambda)$ in the first line depend on R_λ, but approach 1 as R_λ becomes large.

7 The Improved SCT Model

The comparison of theory and data for homogeneous turbulence now produces a much improved Stochastic Closure Model. Namely, the large scale satisfy the equation (4) whereas the small scale flow satisfies the stochastic Navier-Stokes equation,

$$\begin{aligned} du + u\cdot\nabla u dt = &[\nu\Delta u + \nabla(\Delta^{-1}[\mathrm{Trace}(\nabla u)]) - u\cdot\nabla U - U\cdot\nabla u]dt \\ &+ \sum_{k\neq 0}\left(\frac{a}{|a|^2+|k|^m}\right)|k|^{-\frac{5}{3}}dt e_k(x) + \sum_{k\neq 0}\frac{b^{1/2}}{(|b|^2+|k|^m)^{1/2}}|k|^{-1}db_t^k e_k(x) \\ &- u(\frac{1}{3}\sum_{k\neq 0}\bar{N}_t^k dt), \end{aligned} \tag{18}$$

where $a, b^{1/2} \in \mathbb{R}^3$. Here $k \in \mathbb{R}^3$ also. The SCT model now depends on only three parameters $a = |a|$, $b = |b|$ and m that are all function of the Taylor-Reynolds number R_λ. At plot of $1/b$ and $1/a$ for small k and b and a for large k is shown in Figure 7 as functions of the Taylor-Reynolds number. These plots show that the Central Limit part $1/b$ dominates, for k small, and the Large Deviation part a is larger, for k large.

The coefficient C that appears in the computation of the structure functions (15) is not constant for each Taylor-Reynolds number, see Table 4, because it measures both the size of the mean flow and the relative strength of the Center Limit Theorem term and the Large Deviation term in the noise. However, it does not vary much over the center part of Table 4 as a function of the Taylor-Reynolds number. The exponent m also varies because some of the correction terms in (15) absorb its weight and because of the smoothness issue for the higher order structure functions that is discussed below. However, it also does not vary much with the Taylor-Reynolds number above the diagonal in Table 6.

8 Sensitivity Analysis

We now consider the formula for the general p-th structure function as given in (15). If we let the Reynolds Number go to infinity, then the viscosity of the fluid

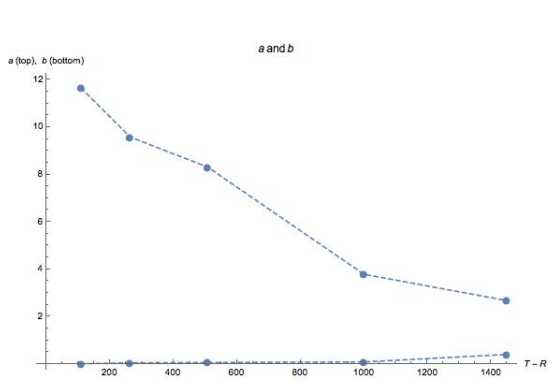

(a) The coefficients a and b.

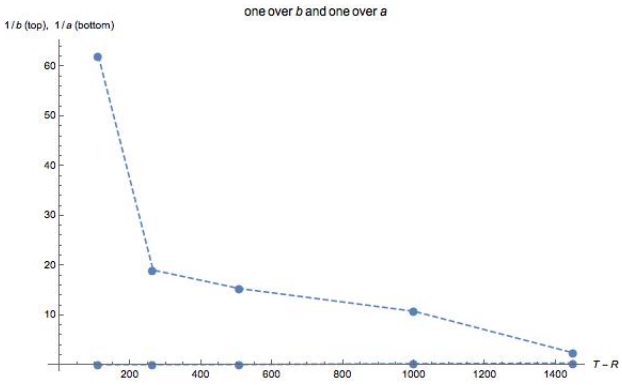

(b) The coefficients 1/b and 1/a (hardly notisable).

Figure 7: The dependence of the coefficients, in the improved SCT model (18), on the Taylor-Reynolds number.

will head to zero. This will simplify the coefficients A_p in (15), for $R_\lambda = \infty$, $\nu = 0$,

$$A_p = \frac{2^{\frac{p}{2}}\Gamma(\frac{p+1}{2})\sigma_k^p {}_1F_1(-\frac{1}{2}p, \frac{1}{2}, -\frac{1}{2}(\frac{M_k}{\sigma_k})^2)}{|k|^{\zeta_p}}. \tag{19}$$

The further denominator terms found in (15) but not above, are corrections to the formula to account for the Reynolds number of the flow. Data fits were also done to the formula without the Reynolds number corrections. Figures 7 to 11 are plots of the error between the formula fits and the data at each data point. The blue circles are the error to the Reynolds corrected formulas while the red diamonds are the error to the formula without the Reynolds number correction.

There are a couple of observations to make about the error plot. First, for small Taylor Reynolds numbers, it appears that the corrections improve the fitting, especially for the smaller data points. This improvement erodes as the Taylor Reynolds number increases, until we see very little difference in accuracy for Taylor Reynolds number 1450. This makes sense, as the corrections to account for Reynolds number get smaller as the Reynolds number increases, with the formulas becoming the uncorrected version when we let the Reynolds number go to infinity.

A second observation may also help explain the issue surrounding the m values of the second structure functions for high Reynolds numbers, discussed in detail below. Table 7 contains the found values for m without the Reynolds number corrections. Here we see a much more pronounced diagonal more in line with

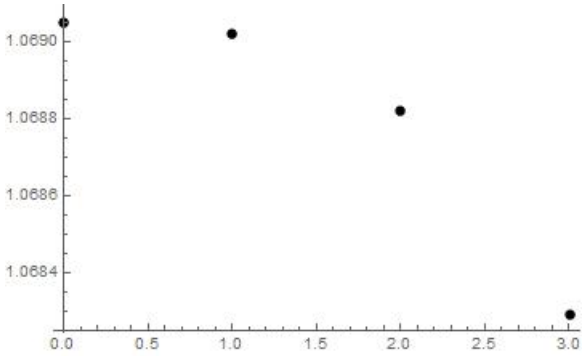

(a) Second Structure Function

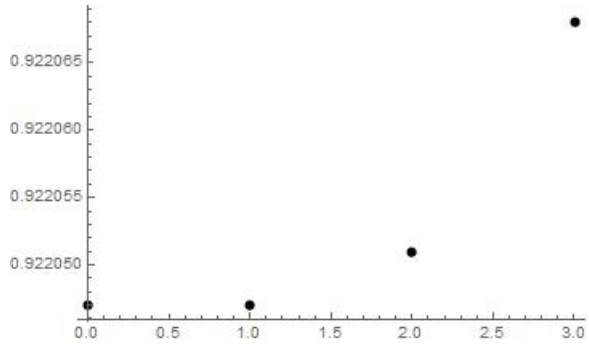

(b) Third Structure Function

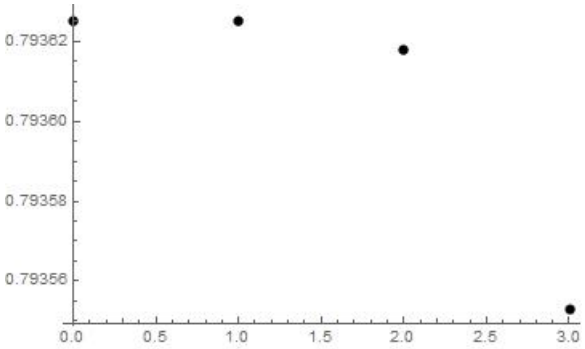

(c) Fourth StructureFunction

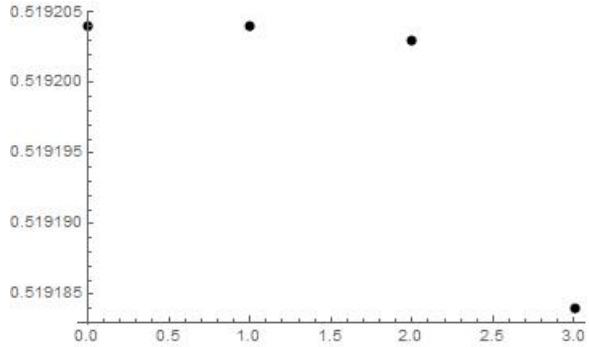

(d) Sixth Structure Function

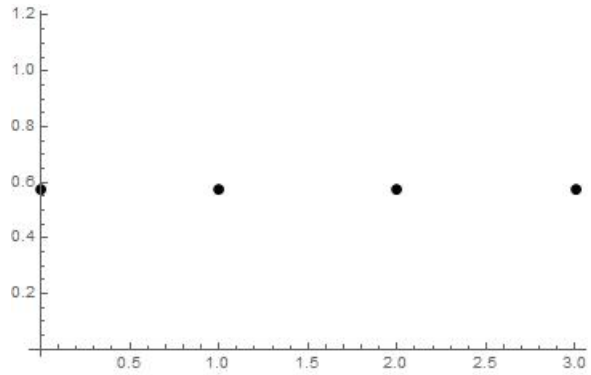

(e) Eighth Structure Function

Figure 8: Robustness test for Reynolds number 508. Note the scales on the y-axis

Taylor Reynolds Number	110	264	508	1000	1450
Second	2.09081	1.49402	1.31448	1.07963	.984291
Third	1.79012	1,41339	1.05553	.822192	.730565
Fourth	1.6408	1.09179	.920749	.687336	.595942
Sixth	1.65727	1.08667	.91658	.681818	.592901
Eighth	1.66164	1.06728	.901549	.662111	.577724

Table 7: The fitted values for m for the uncorrected structure function fits

what the theory predicts. Notice that the Reynolds correction adds the terms

$$\frac{p_k \pi^2 \nu}{C} |k|^{\zeta_p + \frac{4}{3}} + O(\nu^2),$$

to the denominator of the fractions. In particular, this is adding higher powers of k, which may be absorbing some of the power of m, which explains why we see a much more pronounced diagonal form with the exponents when looking at the uncorrected version of the formula in Table 7 than in Table 6 with the corrected version of the formulas.

Finally, we also see an issue in fitting the smallest data points for Reynolds Number 1450. This issue appears to be connected to the system length, as seen in Figure 6. A second fit to the fourth structure function was found with $D = .921$. This does improve the fitting for the smaller data points. However, D being this small causes an issue at the larger data points, namely the sine curve wants to return to zero before the last data point. Since there are relatively few data points at small values of $\frac{r}{\eta}$, we set $D = 1.3$. The value of 1.3 was chosen as it the smallest number needed to fully capture the larger data points.

One potential point of concern with the fitting result was the probe size. The size of the probe could influence the fit and a different probe size could produce different result. To check for this, fits were redone with a reduced number of data points. In particular, for every Taylor Reynolds number and every structure function, fits were redone without including the first, the first two, and the first three data points respectively. We saw minimal change in the main parameters. the greatest being a difference of one in the third significant digit. The robustness test for Reynolds Number 508 are included in Figure 8. As we can see, there is not a significant change in the value of m when removing the first couple of data points. As a result, we are convinced the fits are unaffected by the probe size.

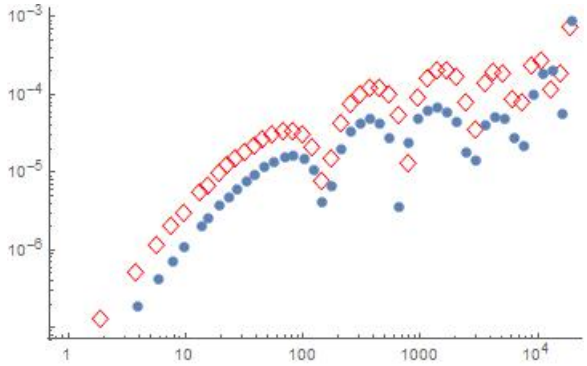

(a) Second Structure Function Error

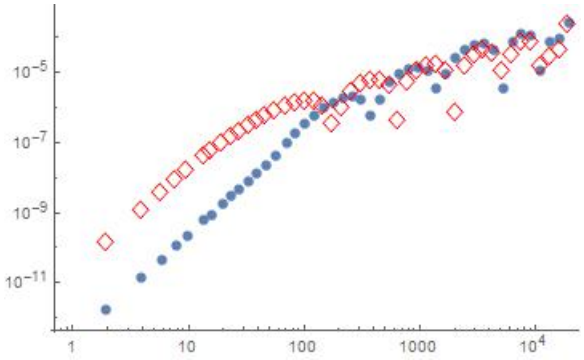

(b) Third Structure Function Error

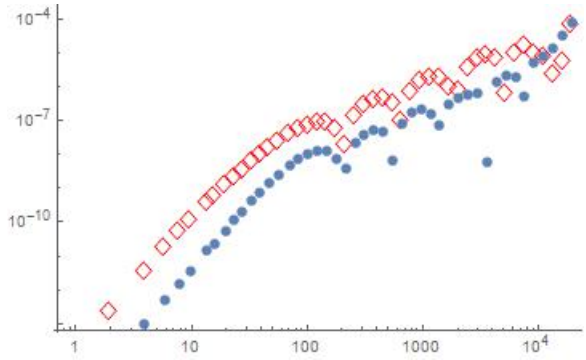

(c) Fourth Structure Function Error

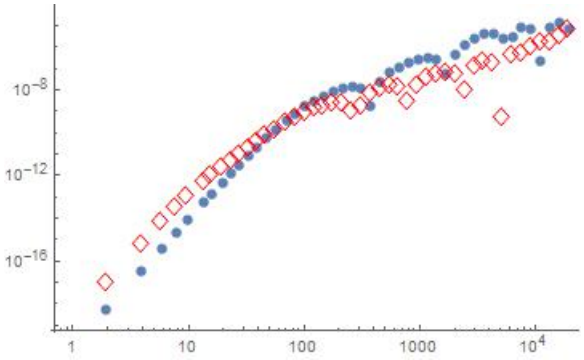

(d) Sixth Structure Function Error

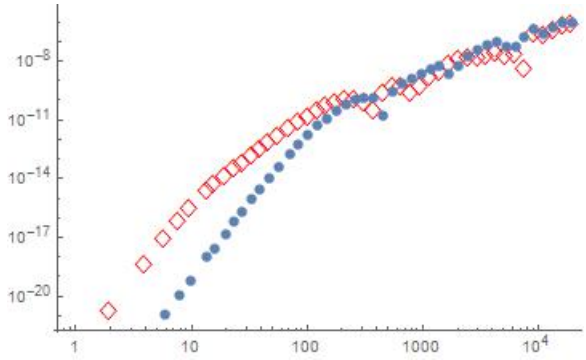

(e) Eighth Structure Function Error

Figure 9: Error for Taylor Reynolds Number 110. Note that the plots are made on a log-log scale. The blue dots are fits to the structure function formula featuring the Reynolds correction whereas the red diamonds are fits to the structure function formula without the Reynolds number correction

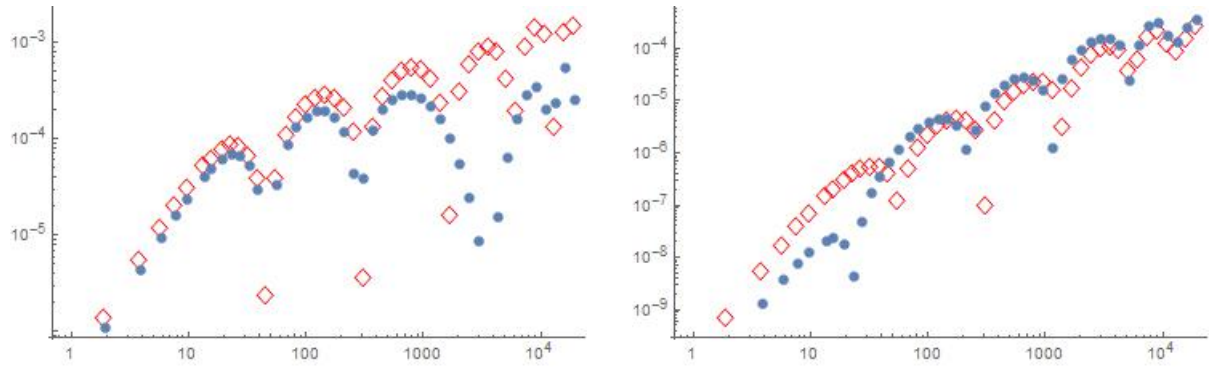

(a) Second Structure Function Error

(b) Third Structure Function Error

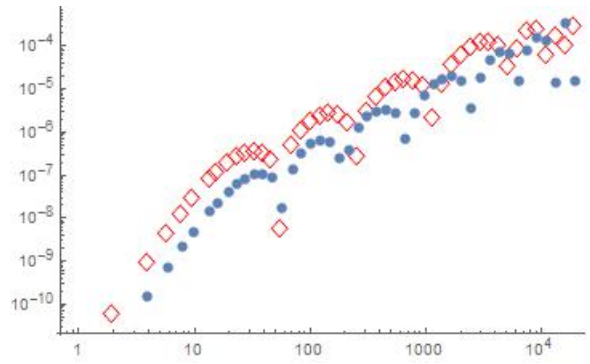

(c) Fourth Structure Function Error

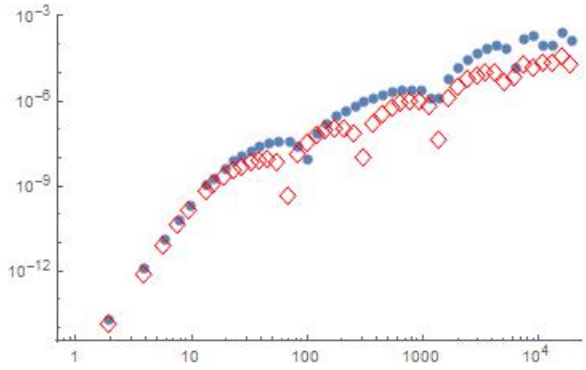

(d) Sixth Structure Function Error

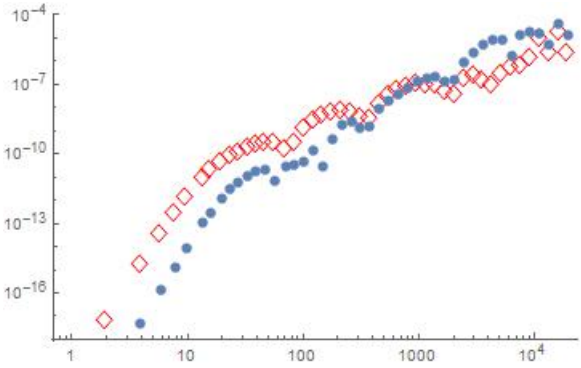

(e) Eighth Structure Function Error

Figure 10: Error for Taylor Reynolds Number 264. Note that the plots are made on a log-log scale. The blue dots are fits to the structure function formula featuring the Reynolds correction whereas the red diamonds are fits to the structure function formula without the Reynolds number correction

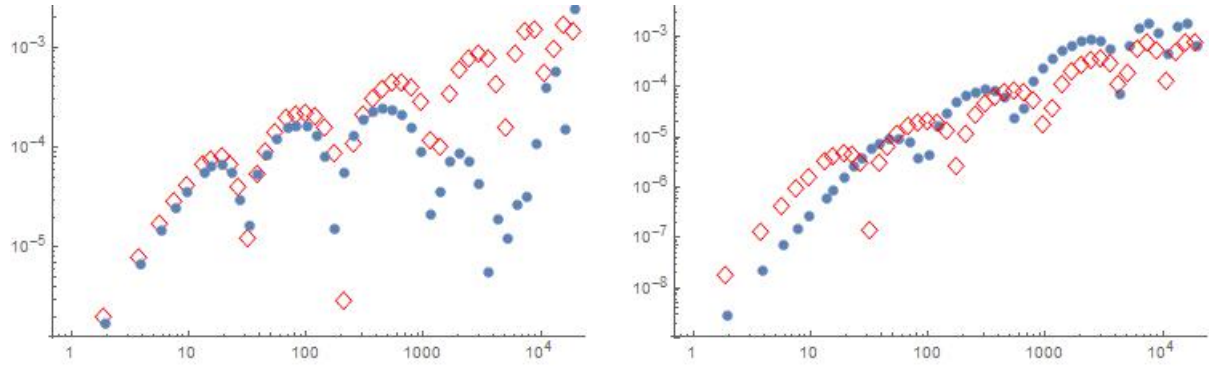

(a) Second Structure Function Error

(b) Third Structure Function Error

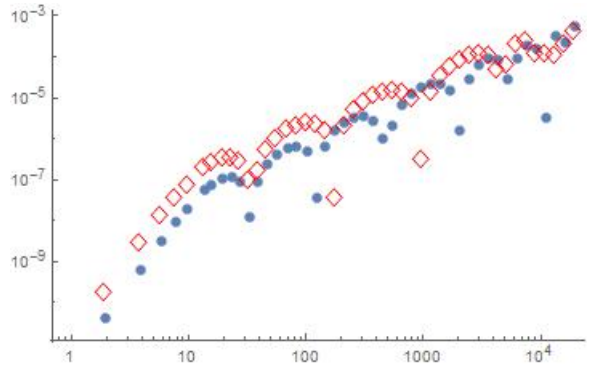

(c) Fourth Structure Function Error

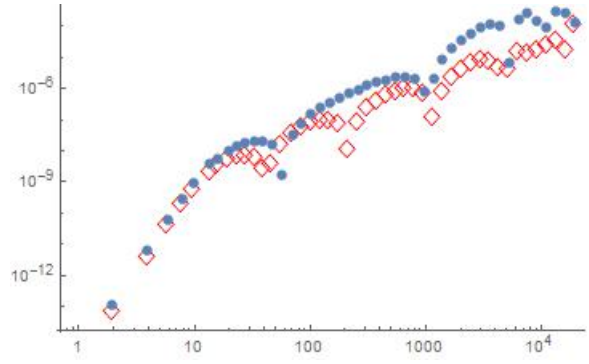

(d) Sixth Structure Function Error

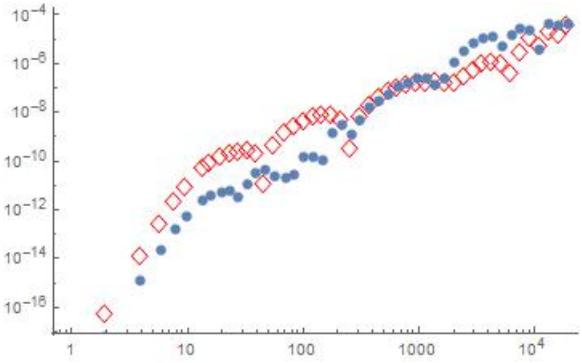

(e) Eighth Structure Function Error

Figure 11: Error for Taylor Reynolds Number 508. Note that the plots are made on a log-log scale. The blue dots are fits to the structure function formula featuring the Reynolds correction whereas the red diamonds are fits to the structure function formula without the Reynolds number correction.

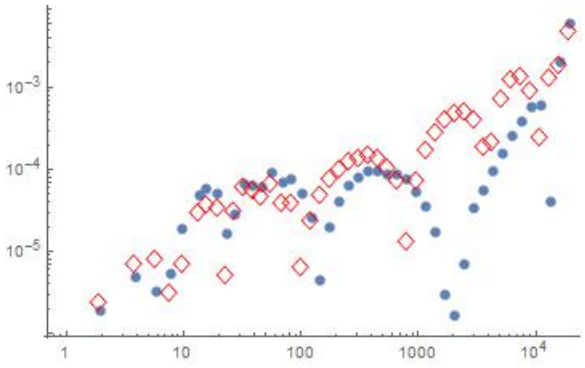

(a) Second Structure Function Error

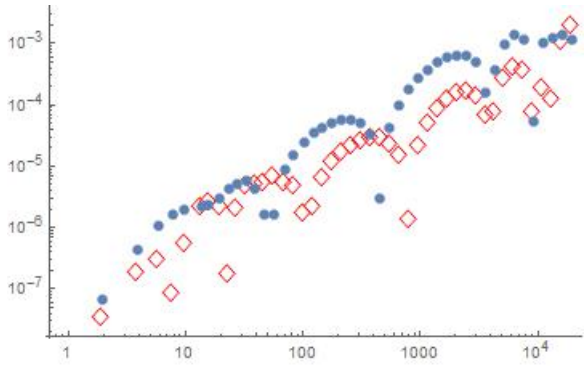

(b) Third Structure Function Error

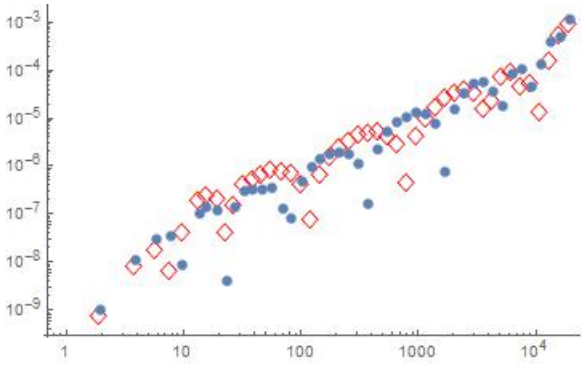

(c) Fourth Structure Function Error

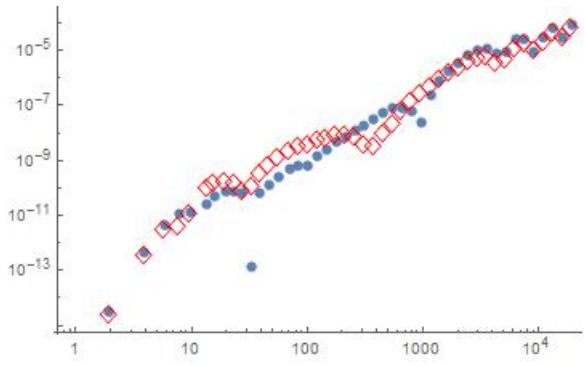

(d) Sixth Structure Function Error

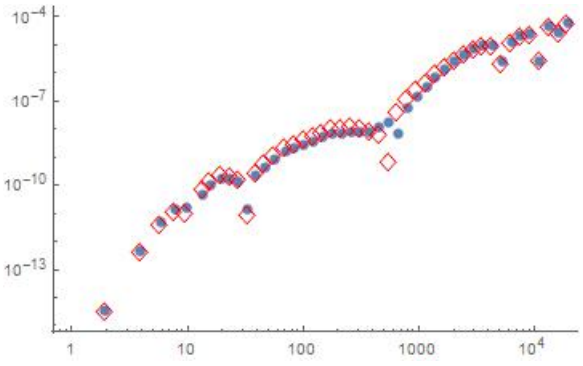

(e) Eighth Structure Function Error

Figure 12: Error for Taylor Reynolds Number 1000. Note that the plots are made on a log-log scale. The blue dots are fits to the structure function formula featuring the Reynolds correction whereas the red diamonds are fits to the structure function formula without the Reynolds number correction.

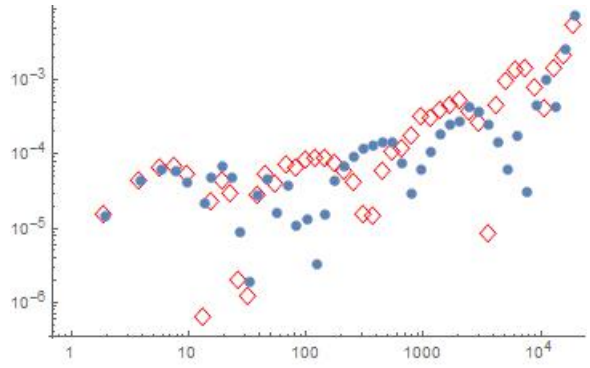

(a) Second Structure Function Error

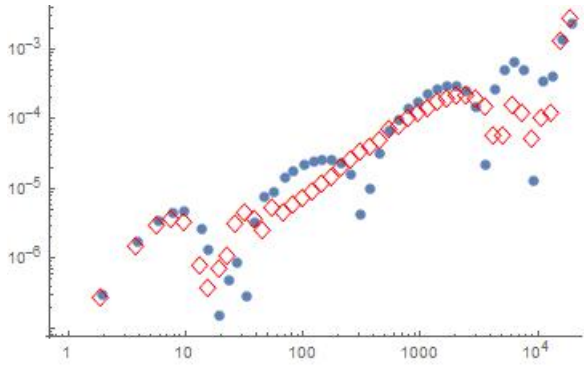

(b) Third Structure Function Error

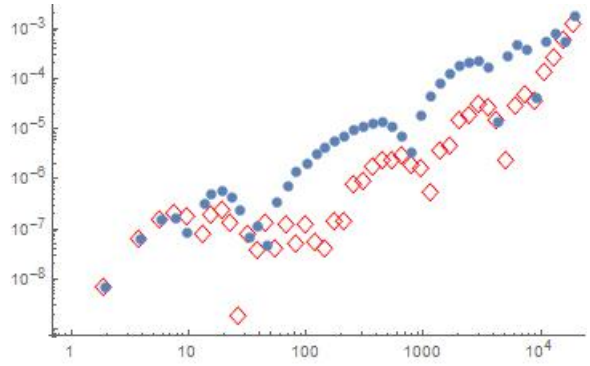

(c) Fourth Structure Function Error

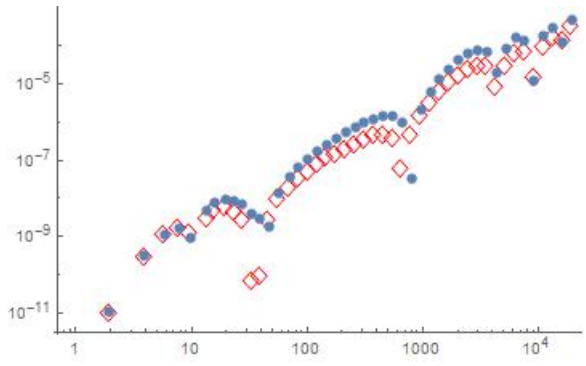

(d) Sixth Structure Function Error

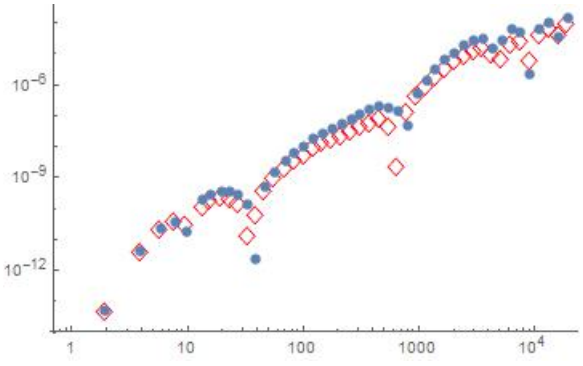

(e) Eighth Structure Function Error

Figure 13: Error for Taylor Reynolds Number 1450. Note that the plots are made on a log-log scale. The blue dots are fits to the structure function formula featuring the Reynolds correction whereas the red diamonds are fits to the structure function formula without the Reynolds number correction.

9 The Smoothness of the Velocity

It was pointed out by Onsager [16, 17] that the fluid velocity in fully turbulent flow could not be a spatially smooth functions, in the limit of infinite Taylor-Reynolds number.

The last line in Table 6, corresponding to the eight structure function, tells an interesting story, that was totally unexpected. There only the exponent for the smallest Reynolds number is close to one. All the other exponents are well below one, the one for the highest Reynolds number going down to 0.248. This seems to contradict the fits for the exponent m from the first line in the Table and the hypothesis on c_k and d_k. In fact, there is a "diagonal" in Table 6, below which the coefficient are well below one, and above which they are larger than one within the fitting uncertainty. The resolution of this apparent contradiction is that the structure functions below the diagonal are not finite in the limit of a very large large Taylor-Reynolds number R_λ and the series (13) representing them do not converge as $R_\lambda \to \infty$. This is what the fits are showing. To explain this we have to discuss the L^p and Sobolev function spaces and the Sobolev inequality, that relates the existence of moments of velocity differences to the differentiability (smoothness) of the turbulent fluid velocity.

The Sobolev inequality can be written as

$$|u|_p \leq C\|u\|_n$$

where $n \geq \frac{3}{2} - \frac{3}{p}$, in three dimensions, and C is a constant. It says that the nth Sobolev space of functions with n derivatives in L^2,

$$\|u\|_n = \sqrt{\sum_{j=0}^{n} |\nabla^j u|_2^2}$$

lies in the space of functions, whose pth moment

$$|u|_p = \left(\int_{\mathbb{R}}^{2} |u|^p dx \right)^{1/p} < \infty$$

is finite. Thus in order for the pth moment (power) of a function to be finite, it is sufficient that it has n derivatives . We apply the Sobolev inequality to the gradient of u below, in order to compare with the moments of the velocity differences δu.

In [6], using Onsager's observation, Birnir showed that the velocity, u, must lie in Sobolev space H^n, where $n = \frac{11}{6}$, when intermittency is not taken into account

and $n = \frac{29}{18}$ when it is. This, in turn, implies that ∇u lies in Sobolev space H^n, where $n = \frac{5}{6}$ without intermittency and $n = \frac{11}{18}$ with intermittency. In order to guarantee convergence of the sine series, we need $H^n \subset L^p$, where p is the number of the structure function. This follows, by the Sobolev inequality, provided that

$$|\nabla u|_p \leq C\|\nabla u\|_n,$$

where C is a constant and $\|\cdot\|_n$ denotes the Sobolev norm, or

$$\frac{5}{6} \geq \frac{3}{2} - \frac{3}{p}.$$

This is true for $p = 2$, $p = 3$ and $p = 4$, but does not hold for $p = 6$ and $p = 8$. Now approximate the velocity differences by the gradient $\delta u \sim \nabla u \cdot r$. Hence, the increase in roughness for the sixth and eighth structure functions agrees with the theory presented by Birnir in [6].

A second issue, indicative of intermittency, arose during the fitting process for the values for m for Taylor Reynolds number 1000 and 1450, see Table 7, where the Taylor-Reynolds number dependence of the structure function has been removed. This prevents the correction terms from absorbing the weight of the exponent m. We mentioned before that m needs to be greater than one in order to ensure convergence. We expect this might not hold for structure functions six and eight for the same reason given in the previous paragraph. However, we get a value less than one for the third and fourth structure functions for Reynolds number 1000 and 1450. While this is by no means a conclusive proof, it may be suggestive of an increasing influence of intermittency as the Reynolds number increases. The inequality $\frac{5}{6} \geq \frac{3}{2} - \frac{3}{p}$ above does not take into account the influence of intermittency. The new inequality when taking intermittency into consideration is

$$\frac{11}{18} \geq \frac{3}{2} - \frac{3}{p}.$$

Now, this is only true $p = 2$ and $p = 3$, but not for $p = 4, 6, 8$, and $p = 3$ is close to the borderline. Hence, the divergence of the series, for the third and fourth structure functions for Taylor Reynolds number 1000 and 1450, may point to an *increasing influence of intermittency* causing a further loss of smoothness in the flow.

10 Conclusion

We started by following Kolmogorov's method as described in Section 2, and formulated in Landau and Lifschitz [15], to close the Navier Stokes equations to describe fully developed turbulence. We did this by introducing a stochastic forcing term to account for the small scales, see [5]. Having closed the model, we then compute a sine series representation for the structure functions of turbulence, with Reynolds number corrections. These formulas were then fitted to data generated from the Variable Density Turbulence Tunnel at the Max Planck Institute for Dynamics and Self-Organization. The fits proved to be very good and yielded valuable insights into the smoothness of the fluid velocity.

For the lower Reynolds number flows, we see convergence of the sine series for the second, third, and fourth structure functions. However, the sixth and eighth structure functions for these Reynolds numbers begin to show sign of divergence. For higher Reynolds number, this divergence becomes more pronounced, as the fourth structure function begins to diverge and the third one begins to show signs of spatial roughness (divergence), as well. This agrees with our theory and may be indicative of an increasing influence of intermittency as the Reynolds number increases.

We compared fits to the formulas for the structure functions with a correction, to account for the Reynolds number, to fits without that correction. We see that the Reynolds correction formulas generate better fits as the Reynolds number decreases for lower structure functions but have little impact on the fits for the higher structure functions. Again, this agrees with theory on the smoothness of the fluid velocity.

The fits simplify the stochastic closure theory (SCT) for the Navier-Stokes equation. We obtain a SCT theory (18) with only three parameters, one corresponding to the variance in the functional Central Limit theorem part of the noise, a second one giving the rate in the Large Deviation part of the noise and finally an exponent that gives the spatial smoothness of the noise (decay in Fourier space). These three parameters depend on the Taylor-Reynolds number but are independent of the order of the structure functions.

References

[1] John D Anderson Jr. *A history of aerodynamics: and its impact on flying machines*, volume 8. Cambridge University Press, 1999.

[2] Donald D Baals and William R Corliss. *Wind tunnels of NASA*, volume 440. Scientific and Technical Information Branch, National Aeronautics and Space Administration, 1981.

[3] O. E. Barndorff-Nilsen. Exponentially decreasing distributions for the logarithm of the particle size. *Proc. R. Soc. London*, A 353:401–419, 1977.

[4] P. S. Bernard and J. M. Wallace. *Turbulent Flow*. John Wiley & Sons, Hoboken, NJ, 2002.

[5] B. Birnir. The Kolmogorov-Obukhov statistical theory of turbulence. *J. Nonlinear Sci.*, 2013. DOI 10.1007/s00332-012-9164-z.

[6] B. Birnir. *The Kolmogorov-Obukhov Theory of Turbulence*. Springer, New York, 2013.

[7] Björn Birnir. *From Wind-Blown Sand to Turbulence and Back*, pages 15–27. Springer International Publishing, Cham, 2016.

[8] Eberhard Bodenschatz, Gregory P Bewley, Holger Nobach, Michael Sinhuber, and Haitao Xu. Variable density turbulence tunnel facility. *Review of Scientific Instruments*, 85(9):093908, 2014.

[9] Genevieve Comte-Bellot and Stanley Corrsin. The use of a contraction to improve the isotropy of grid-generated turbulence. *Journal of Fluid Mechanics*, 25(04):657–682, 1966.

[10] S Corrsin. Turbulent flow. *American Scientist*, 49(3):300–325, 1961.

[11] B. Dubrulle. Intermittency in fully developed turbulence: in log-Poisson statistics and generalized scale covariance. *Phys. Rev. Letters*, 73(7):959–962, 1994.

[12] A. N. Kolmogorov. Dissipation of energy under locally istotropic turbulence. *Dokl. Akad. Nauk SSSR*, 32:16–18, 1941.

[13] A. N. Kolmogorov. The local structure of turbulence in incompressible viscous fluid for very large Reynolds number. *Dokl. Akad. Nauk SSSR*, 30:9–13, 1941.

[14] A. N. Kolmogorov. A refinement of previous hypotheses concerning the local structure of turbulence in a viscous incompressible fluid at high Reynolds number. *J. Fluid Mech.*, 13:82–85, 1962.

[15] Lev Davidovich Landau and Evgenii Mikhailovich Lifshits. *Fluid Mechanics: Transl. from the Russian by JB Sykes and WH Reid*. Addison-Wesley, 1959.

[16] L. Onsager. The distribution of energy in turbulence. *Phys. Rev.*, 68:285, 1945.

[17] L. Onsager. Statistical hydrodynamics. *Nuovo Cimento.*, 6(2):279–287, 1945.

[18] S. B. Pope. *Turbulent Flows*. Cambridge Univ. Press, Cambridge UK, 2000.

[19] Ludwig Prandtl. Göttingen wind tunnel for testing aircraft models, 1920.

[20] O. Reynolds. On the dynamical theory of incompressible viscous fluids and the determination of the criterion. *Phil. Trans. Roy. Soc. Lond.*, 186A:123–164, 1885.

[21] Z-S She and E. Leveque. Universal scaling laws in fully developed turbulence. *Phys. Rev. Letters*, 72(3):336–339, 1994.

[22] Z-S She and E. Waymire. Quantized energy cascade and log-poisson statistics in fully developed turbulence. *Phys. Rev. Letters*, 74(2):262–265, 1995.

[23] G. I. Taylor. Statistical theory of turbulence. *Proc. Royal Soc. London*, 151:421–444, 1935.

[24] J. B. Walsh. *An Introduction to Stochastic Differential Equations*. Springer Lecture Notes, eds. A. Dold and B. Eckmann, Springer, New York, 1984.